Spatial-temporal trends mapping (GWD) and Geostatistical modelling of Groundwater level depth over Northern parts of Indo-Gangetic Basin, India

Abstract

Haryana-Punjab is a vast part of the Indo-Gangetic basin (India), recognised globally as a major hotspot of groundwater abstraction and agricultural economic reliance. A lack of information is present in this region regarding spatiotemporal changes in groundwater levels. Geostatistical anisotropic processes are reliable, especially when the monitored regions are extensive. The modelling study involves a twofold objective. First, it estimates and evaluates anisotropic spatial variations in groundwater level depth (GWD, Surface to water level) using geostatistics for all four seasons of Indian cropping patterns—pre-monsoon, monsoon, post-monsoon (rabi) and post-monsoon (Kharif), and parameters of point kriging cross-validation (PKCV) are optimum, acceptable, and support the unbiasedness hypothesis of kriging. Based on the PKCV, five essential parameters were computed to accept the anisotropy semi-variogram fitted model. These are (1) kriging mean error (KME), ideally close to zero so that there are no over or underestimates, (2) goodness of fit (R^2), (3) the ratio of estimated variance (EV) to kriging variance (KV) lies between 0.95-1.05, (4) good eye visualisation fit and (5) significant t-test on the correlation coefficient. The second objective is spatiotemporal modelling, a pixel-based Mann-Kendall trend testing (at 95% Confidence Interval) on kriged raster surfaces of GWD (For all four seasons) at 1km grid resolution. The trend, significant or not, is determined by the Mann-Kendall test, while Sen's slope estimator determines the slope magnitude of the trend. Results revealed that the study area's east-central to the central-northern region comes under a high depletion zone for groundwater levels. GWD significantly increased by 120cm/year-80cm/year in this region, and the mean kriged GWD for the entire study area increased by 30cm/year-29cm/year over 25 years**.** Seasonal climatological mean maps of kriged surfaces of GWD and mean rainfall surfaces in two different time phases for all four seasons have been evaluated. It is observed from these maps that wherever the rainfall is increasing, GWD is decreasing. Results clarified that anisotropic semi-variogram modelling with kriging, pixel-based trend analysis, and regression studies is a valuable tool for identifying the critical region of groundwater levels, and the central region of the study area falls under the severe depletion condition of the groundwater level.

Keywords: PKCV, kriging, significant trend, Mann-Kendall, Sen's slope.

1 Introduction

Groundwater is one of the most valuable and vital natural resources for the survival of human life. The Indo-Gangetic basin's aquifer system is one of the world's most valuable groundwater resources, and the agricultural economy of these regions is mainly dependent on groundwater irrigation systems (MacDonald et al., 2016). The expansion of agricultural areas and primary reliance on groundwater abstraction have significantly declined groundwater in this aquifer system (Gleeson et al., 2020). The northern part of India, like Haryana-Punjab (Part of the Indo-Gangetic basin), has been recognized globally as a significant zone of groundwater crisis (Joshi & Gupta, 2021; Rodell et al., 2009; MacDonald et al., 2016). This area has become the leading area where a rapid decrease in groundwater level is observed (Siebert et al., 2010; Shankar et al., 2011; Saha et al., 2018). Moreover, the livelihood of the inhabitants depends on cultivation, groundwater resources, and surface water (Sarkar, 2012). If this tendency proceeds and the groundwater monitoring system in this region does not get attention, severe damage will affect the aquifer's body (Singh R.B., 2001). Understanding the long-term spatial-temporal variation of groundwater levels and rainfall provides an effective tool for exploring possible groundwater zones and is essential for the best monitoring of groundwater resources (Nourani et al., 2008; Rajmohan et al., 2006). The geographical boundaries of the study area enclosed the coordinates of 35.50^0, 6.75^0 (latitude), and 68.180, 97.410 (longitude), and the total aerial extent is 96918.41 km^2. Haryana and Punjab regions are covered by a large expanse of quaternary sediments of alluvial and aeolian origin, and these areas are surrounded by hard rocks (Chopra & Sharma, 1993; Srivastava et al., 2014) in the northeastern part (Tertiary) of the region to the southwestern margin (Archean rock). The study area was divided into three geomorphic units (Kale, 2002; Srivastava et al., 2006). First, the high structural hills exist in the study area's extreme northwest corner and fall at the margin of Himachal Pradesh. Second is the moderate structural denudation hills; this geomorphic part is restricted to the study area's northeastern section and mainly composed of rocks with moderate relief topography. Third, the area is exposed on the northeastern boundary of Haryana state; this region is mainly confined to the low structural denudational hills (Srivastava et al., 2014). The present study aims to understand rainfall and groundwater levels' long-term seasonal spatial-temporal behaviour and identify the critical and safe zone with a minimum error factor. *Geostatistics* is the method that provides the kriged map with an uncertainty (kriging variance) map. This technique is based on the doctrine of regionalized variables (Machiwal et al., 2012; Uyan & Cay, 2013). Kriging with anisotropy and pixel-based trend modelling (Mann-Kendall significant test) are advanced approaches to understanding groundwater levels (Neeti et al., 2011).

2. Materials and Methods

2.1 Data

Two sorts of data are use in the present research thrust. The first data is the groundwater level depth (GWD), and the second is the remote sensing satellite rainfall data (Tropical Rainfall Measuring Mission, 25km grid resolution) from 1996 to 2020 and 1998 to 2019, respectively. Rainfall and GWD data are arranged according to India's seasonal cropping patterns. These seasons are pre-monsoon (March-May), monsoon (June-August), post-monsoon rabi (November-December), and post-monsoon kharif (September-October) (http://cgwb.gov.in). GWD data is inconsistent for the time series 1996 to 2020, and box plots in Figure 5.2 show these missing years for GWD.

Geostatistical modeling

The first methodology employed was the geostatistical modeling of GWD for all four seasons in each year (1996-2020). When spatial dependence (autocorrelation) is more robust in one direction than another, detect anisotropy in the data set. The most common techniques for assessing isotropy/anisotropy are directional semi-variogram and variogram surface (Mateu, J. et al., 2008). The present study deals with the anisotropy analysis of semi-variograms because the study area is very large, and the autocorrelation of the GWD data are found different in different direction. Among all forms of spatial anisotropy, geometric and zonal anisotropy is most common. The Sill (Nugget + Continuity) value of the Geometric anisotropic variogram only varies along with distances (Range) while for Zonal anisotropic variogram the sill varies along with all distances and directions. Natural phenomena like geological, atmospheric changes, etc., usually have the combination of Geometric and Zonal anisotropy. When the nugget variance is not too significant but important with a clear range and sill, then a spherical model of semi-variogram is a good selection among other semi-variogram models (Isaaks & Srivastava, 1989). Once get the values of Sill, Range, Nugget from all variograms, determine the spatial data is isotropic or anisotropic by the process of exploratory data analysis (EDA) (Manto, H., 2005). The anisotropic variogram model is the function of "distance" and "direction," and the equation is shown as follows (Equation 1):

$$\Upsilon(h,\Theta)=\frac{1}{2}\{N(h,\Theta)\}\sum_{i=1}^{N(h,\Theta)}[Z(xi)-Z(xi+h,\Theta)]^2 \quad \text{---------- (1)}$$

Where Θ is the angle along point x_i and $x_{i+h,}$ N (h, Θ) pairs of samples with interval "h" in the angles along point x_i and x_{i+h}. If there are two regionalized variables "z" and "y", the joint variogram could be obtained via:

$$\Upsilon_{zy}(h)= 1/2N(h)\sum_{i=1}^{N(h)}[Z(xi)-Z(xi+h)]*[y(xi)-y(xi)-y(xi+h)]^2 \text{----------(2)}$$

The most appropriate semi-variogram model is chosen on a trial-and-error basis of the point kriging cross-validation (PKCV) technique. Based on the PKCV, five essential parameters were computed to accept the anisotropy semi-variogram model. These are (1) kriging mean error (KME) ideally close to zero so that there is no over or underestimates (Giraldo et al., 2011), (2) goodness of fit (R^2), (3) the ratio of estimated variance (EV) to kriging variance (KV) lies between 0.95-1.05 (Saikia & Sarkar, 2013) (4) good eye visualization fit and (5) significant t-test on the correlation coefficient (Edgell et al.,1984). Among the various ways of kriging, this part of the present research deals with ordinary kriging. Let G* be the kriged estimate of the mean value of grid G of the samples having values g_1, g_2, g_3……g_n and let a_1, a_2, a_3……a_n be the weightage giving to each of the values respectively such that $\Sigma a_i=1$; and $G^*=\Sigma a_i g_i$. Thus the estimation becomes unbiased; the mean error is zero for a large number of estimated values, and the kriging variance or standard error (equation 3 & 3.1) is given as:

$$\sigma_k^2 = \Sigma (G_i - G^*)^2 \quad \text{---------- (3)}$$

$$\text{Kriging standard error} = \sqrt{\sigma_k^2} \text{------ (4)}$$

A coefficient is called Lagrange multiplier (□) (equation 4), used for the optimal solution of the kriging matrix. To achieve the condition of unbiased estimations of ordinary Kriging, the following set of equations have to be solved concurrently:

$$\begin{cases} \sum_{i=1}^{n} \lambda i \Upsilon(h,\Theta) - \square = \Upsilon(h,\Theta) \\ \sum_{i=1}^{n} \lambda i = 1 \end{cases} \text{---------- (4)}$$

Where λi is the weight associated with the data.

2.2 Mann-Kendall Trend Modelling and Sen's slope

The second modeling work employed was a pixel-based Mann-Kendall (M.K.) trend modeling (Neeti & Eastman, 2011) on kriged raster surfaces of GWD. The statistical significance of the trend was analyzed using the M.K. test and the magnitudes of the trend were estimated using Sen's slope estimator (Sobrino & Julien, 2013). Sen's slope's positive and negative value indicates an upward and downward trend, respectively (Gajbhiye, S et al., 2016). Sen's slope estimator (Sen, P. K., 1968) was applied to each pixel of kriged raster GWD for estimating the slope of trend in the kriged raster surfaces of GWD to quantify the magnitude of the trend associated. The advantage of this test is that it is not affected by missing data and need not conform to any specific distribution (Jaagus, 2006). This non-parametric test null hypothesis (Ho) tells that in an "n" samples value of the data set (x_1 …, x_n) is identically and independently distribution of random variables. This test's alternative hypothesis (H1) states that the distributions of x_k and x_j are not identical for all k and $j \leq n$ with $k \neq j$. M.K. test statistics denoted by S, having zero mean and a variance estimated by equation (3) is given by;

$$S = \sum_{i=1}^{n-1} \sum_{j=i+1}^{n} \text{sgn}\,(xj - xk) \text{---------- (1)}$$

Where xj and xk represent n data points at times j and k respectively, and sgn is the sign function defined by:

$$\text{sgn} = \begin{cases} 1 & \text{if } (xj - xi) > 0 \\ 0 & \text{if } (xj - xi) = 0 \\ -1 & \text{if } (xj - xi) < 0 \end{cases} \text{---------- (2)}$$

For higher values of n, where n>= 10, the M.K. test statistics S follows the approximately normal distribution with mean as zero and variance V(s) as computed by equation (3):

$$V(s) = n(n-1)(2n+5) - \sum_{j=1}^{p} tj(tj-1)(2tj+5)/18 \text{ --------- (3)}$$

Where n refers to the number of data points, tj specifies the number of data points in the pth group. Tied groups (a tied group is a set of sample data having the same value) represented are by p. tj is the number of data points in the jth tied groups (Da Silva et al., 2015). The probability associated with S (equation 1 & 2) and the sample size n statistically computed were to quantify the significance of the trend. Then, the normalized test statistics Zak computes using equation (4) as given below:

$$Z_{mk} = \begin{cases} \frac{S-1}{\sqrt{\text{var}\,(s)}}, & \text{when } s > 0 \\ 0, & \text{when } s = 0 \\ \frac{S-1}{\sqrt{\text{var}\,(s)}}, & \text{when } s < 0 \end{cases} \text{---------- (4)}$$

The null hypothesis is rejected at a 90% confidence level if the p-value ≥ 0.10. The resulting trend may have any of the three values (equation 4), i.e., positive, negative, or zero (no trend), with a corresponding confidence level based on the p-value (Yusuf et al., 2018).

3. **Results**

Geostatistical modelling involving a spatial correlation study of the geo-variables (GWD) was carried out through an anisotropy-fitted semi-variogram model (Figure 1). Spatial variability modelling was first implemented with the computation of crude anisotropy semi-variograms and then fitting suitable mathematical models (Figure 1) that characterized the spatial variability of GWD. The modelling study revealed that all parameters of PKCV (Table 1a & b) denote the best-accepted fitted model for the anisotropic spherical semi-variogram. Geostatistical estimation

commenced with gridding the boundary area of the study region into cells 1000mX1000m, with each cell defined in space in terms of northing and easting. Ordinary kriging (OK) has been carried out for each grid cell, which generated a kriged estimate and associated kriging standard error concerning all four seasons of GWD. Spatial variability maps of kriged estimate values concerning all four seasons of kriged GWD exhibit a significant difference in starting (1996 for all seasons) and ending year (2019 for pre-monsoon, 2020 for other seasons) (Figure 2). For all four seasons, the starting year of kriged GWD varies from 1 to 10 meters, but for the ending year, kriged GWD varies from 10-30 meters and is distinctly high in the central region of the study area. The Kriging standard error maps exhibit a relatively high error in the study area's north-eastern-central, southern and eastern peripheries due to a significantly lower density of wells (sample location).

In contrast, in the rest of the parts, the error reduces towards the areas with many wells as prominently present in the south-western part to the eastern and some of the north. The grid resolution of the TRMM rainfall raster is 25 km x 25 km, and it is dragged to 1000mX1000m by GIS modelling. Seasonal climatological mean maps of kriged surfaces of GWD and mean rainfall surfaces in two different time phases for all four seasons (Pre-monsoon (1998-2019 & 1998-2008), monsoon (1998-2019 & 1998-2008), post-monsoon-rabi (1998-2018 & 1998-2008), post-monsoon-kharif (1998-2018 & 1998-2008)) have been shown in Figure from 3(a) to 3(d). It is observed from mean climatological maps of GWD and rainfall that wherever the rainfall is increasing, GWD is also increasing. Results revealed that the high rainfall catchment area is significant for the time phase 1998-2008 for pre-monsoon and monsoon seasons compared to the second time phase (1998-2019) for the same seasons (Pre-monsoon & Monsoon, Figure 3(a) & 3(b). Similarly, the catchment area for the high value of climatological mean kriged GWD shows a decreasing trending pattern for all seasons from the first time phase ((Pre-monsoon (1998-2008), monsoon (1998-2008), post-monsoon-rabi (1998-2008), post-monsoon-kharif (1998-2008))) compared to the second time phase ((Pre-monsoon (1998-2019), monsoon (1998-2019), post-monsoon-rabi (1998-2017), post-monsoon-kharif (1998-2018))for all seasons (Figure 3(a) to 3(d). Pixel-based MK (at 90% C.I.) trend modelling is shown in Figures 5a and 5b. Based on the time range (1996-2019 for pre-monsoon and 1996-2020 for other seasons) of the trends maps and Sen's slope values, the slope of kriged GWD is divided into four zones. The first zone is a high-restoration zone (HRZ), where Sen's slope ranges between -30 cm/year to -20 cm/year. The second zone is a low-restoration zone (LRZ), where the range of Sen's slope is -20 cm/year to 0 cm/year. The third and the fourth zones are low-rate depletion zone (LDZ), and high-rate depletion zones (HDZ) and significant Sen's slope range at 90% C.I. for LDZ is 0 - 40 cm/year, while the HDZ zone is 40cm/year - 120cm/year. The mean significant Sen's slope of GWD of all four seasons for HDZ lies between 50cm/year and 55 cm/year, and the range for HRZ is -22 cm/year to 23cm/year (Figures 5a and 5b). A statistical explanation of input raw data of GWD and rainfall is shown from the box plots (Figure 4a & 4b). It is revealed from the box plot of GWD, that a higher anomaly is observed for the years 2018, 2019 and 2020.

5. Discussion and Conclusions

It is essential to understand the seasonal behaviour of GWD and rainfall concerning a vast space and time domain area. The study focuses on long-term, high-resolution GWD and rainfall in the part of the Indo-Gangetic region (Haryana & Punjab). Results reveal distinct patterns of GWD and rainfall that have yet to be uniform across the study area. The climatological mean maps (Figure 3(a) to 3.(d) of kriged GWD found a significant groundwater depletion zone central to

the study area's northern region. Kriging standard error maps for GWD revealed that more wells are needed in the study area's southern, northern, and eastern periphery and some parts of the central region. Kriged surface generation of GWD and trend modelling revealed spatiotemporal variations in the GWD in the study area. Pixel-based trend results on kriged raster GWD at 90% C.I. revealed that in the east-central to central-northern region, GWD is significantly increasing. Kaithal, Karnal, Bathinda, Barnala, Jind, Fatehgarh Sahibzada, Tarn Taran, and Hoshiarpur districts come under HDZ, and the mean Sen's slope in this region significantly increases with the rate of 52cm/year-57cm/year (Figure 5a & 5b). However, the periphery of the study area comes under the zone of HRZ and LRZ, and the mean Sen's slope of GWD in these regions is significantly declining at the rate of -20cm/year to -6cm/year (Figure 5a & 5b). The comprehensive study concluded that the east-central to central-northern zones of the study area are critical conditions for groundwater levels (Mean Sea Level). Less rainfall was observed in this region in comparison to other zones. A regression study was also conducted on the mean kriged GWD of all four seasons and revealed that the mean kriged GWD for the entire study increased at the rate of 29cm/year to 30cm/year over 24-25years for all four seasons (Figure 5a & 5b). The regression studies' coefficient of determination (R^2) lies between 0.70 and 0.62, which is an adverse impact on the aquifer of the study area. Results clarified that anisotropic semi-variogram modelling with kriging, pixel-based trend analysis, and regression studies is a valuable tool for identifying the critical region of groundwater levels that needs more attention for sustainable groundwater treatment and the central region of the study area falls under the severe depletion condition of the groundwater level.

COMPETING INTERESTS

Authors have declared that they have no known competing financial interests OR non-financial interests OR personal relationships that could have appeared to influence the work reported in this paper.

References

Chopra, R., & Sharma, P. K. (1993). Landform analysis and ground water potential in the Bist Doab area, Punjab, India. *International Journal of Remote Sensing*, *14*(17), 3221-3229.

Da Silva, R. M., Santos, C. A., Moreira, M., Corte-Real, J., Silva, V. C., & Medeiros, I. C. (2015). Rainfall and river flow trends using Mann–Kendall and Sen's slope estimator statistical tests in the Cobres River basin. *Natural Hazards*, *77*(2), 1205-1221.

Edgell, S. E., & Noon, S. M. (1984). Effect of violation of normality on the t test of the correlation coefficient. *Psychological bulletin*, *95*(3), 576.

Gajbhiye, S., Meshram, C., Mirabbasi, R., & Sharma, S. K. (2016). Trend analysis of rainfall time series for Sindh river basin in India. *Theoretical and applied climatology*, *125*(3), 593-608.

Giraldo, R., Delicado, P., & Mateu, J. (2011). Ordinary kriging for function-valued spatial data. *Environmental and ecological statistics*, *18*(3), 411-426.

Gw Year Book 2019-20 All India Final 752021. Retrieved from http://cgwb.gov.in/Ground-Water/GW YEAR BOOK 2019-20 ALL INDIA FINAL 752021 (1).pdf

Isaaks, E. H., & Srivastava, R. M. (1989). An introduction to applied geostatistics: Oxford University Press, 561. *Search in*.

Jaagus, J. (2006). Climatic changes in Estonia during the second half of the 20th century in relationship with changes in large-scale atmospheric circulation. *Theoretical and Applied Climatology*, *83*(1), 77-88.

Joshi, S. K., Gupta, S., Sinha, R., Densmore, A. L., Rai, S. P., Shekhar, S., ... & van Dijk, W. M. (2021). Strongly heterogeneous patterns of groundwater depletion in Northwestern India. *Journal of hydrology*, *598*, 126492.

Kale, V. S. (2002). Fluvial geomorphology of Indian rivers: An overview. *Progress in Physical Geography*, *26*(3), 400–433. https://doi.org/10.1191/0309133302pp343ra

MacDonald, A. M., Bonsor, H. C., Ahmed, K. M., Burgess, W. G., Basharat, M., Calow, R. C., ... & Yadav, S. K. (2016). Groundwater quality and depletion in the Indo-Gangetic Basin mapped from in situ observations. *Nature Geoscience*, *9*(10), 762-766.

MacDonald, A. M., Bonsor, H. C., Ahmed, K. M., Burgess, W. G., Basharat, M., Calow, R. C., ... & Yadav, S. K. (2016). Groundwater quality and depletion in the Indo-Gangetic Basin mapped from in situ observations. *Nature Geoscience*, *9*(10), 762-766.

Machiwal, D., Mishra, A., Jha, M. K., Sharma, A., & Sisodia, S. S. (2012). Modeling short-term spatial and temporal variability of groundwater level using geostatistics and GIS. *Natural resources research*, *21*(1), 117-136.

Manto, H. (2005). Modelling of geometric anisotropic spatial variation. *Mathematical Modelling and Analysis*, 361-366.

Mateu, J., Porcu, E., & Gregori, P. (2008). Recent advances to model anisotropic space–time data. *Statistical Methods and Applications*, *17*(2), 209-223.

Neeti, N., & Eastman, J. R. (2011). A contextual mann- kendall approach for the assessment of trend significance in image time series. *Transactions in GIS*, *15*(5), 599-611.

Nourani, V., Mogaddam, A. A., & Nadiri, A. O. (2008). An ANN- based model for spatiotemporal groundwater level forecasting. *Hydrological Processes: An International Journal*, *22*(26), 5054-5066.

Rajmohan, N., & Elango, L. (2006). Hydrogeochemistry and its relation to groundwater level fluctuation in the Palar and Cheyyar river basins, southern India. *Hydrological Processes: An International Journal*, *20*(11), 2415-2427.

Rodell, M., Velicogna, I., & Famiglietti, J. S. (2009). Satellite-based estimates of groundwater depletion in India. *Nature*, *460*(7258), 999-1002.

Saha, D., Marwaha, S., & Mukherjee, A. (2018). Groundwater resources and sustainable management issues in India. In *Clean and sustainable groundwater in India* (pp. 1-11). Springer, Singapore.

Saikia, K., & Sarkar, B. C. (2013). Coal exploration modelling using geostatistics in Jharia coalfield, India. *International Journal of Coal Geology*, *112*, 36-52.

Sarkar, A. (2012). Sustaining livelihoods in face of groundwater depletion: a case study of Punjab, India. *Environment, development and sustainability*, *14*(2), 183-195.

Sen, P. K. (1968). Estimates of the regression coefficient based on Kendall's tau. *Journal of the American statistical association*, *63*(324), 1379-1389.

Shankar, P. V., Kulkarni, H., & Krishnan, S. (2011). India's groundwater challenge and the way forward. *Economic and political Weekly*, 37-45.

Siebert, S., Burke, J., Faures, J. M., Frenken, K., Hoogeveen, J., Döll, P., & Portmann, F. T. (2010). Groundwater use for irrigation–a global inventory. *Hydrology and earth system sciences*, *14*(10), 1863-1880.

Singh, R. B. (2001). Impact of land-use change on groundwater in the Punjab-Haryana plains, India. *IAHS PUBLICATION*, 117-122.

Sobrino, J. A., & Julien, Y. (2013). Trend analysis of global MODIS-Terra vegetation indices and land surface temperature between 2000 and 2011. *IEEE Journal of Selected Topics in Applied Earth Observations and Remote Sensing*, *6*(5), 2139-2145.

Srivastava, G. S., Singh, I. B., & Kulshrestha, A. K. (2014). Geomorphic and Tectonic features of Punjab-Haryana Plain as identified from digital elevation model and surface profiles. *Him Geol*, *35*(2), 97-109.

Uyan, M., & Cay, T. (2013). Spatial analyses of groundwater level differences using geostatistical modeling. *Environmental and ecological statistics*, *20*(4), 633-646.

Yusuf, A. S., Edet, C. O., Oche, C. O., & Agbo, E. P. (2018). Trend analysis of temperature in Gombe state using Mann Kendall trend test.

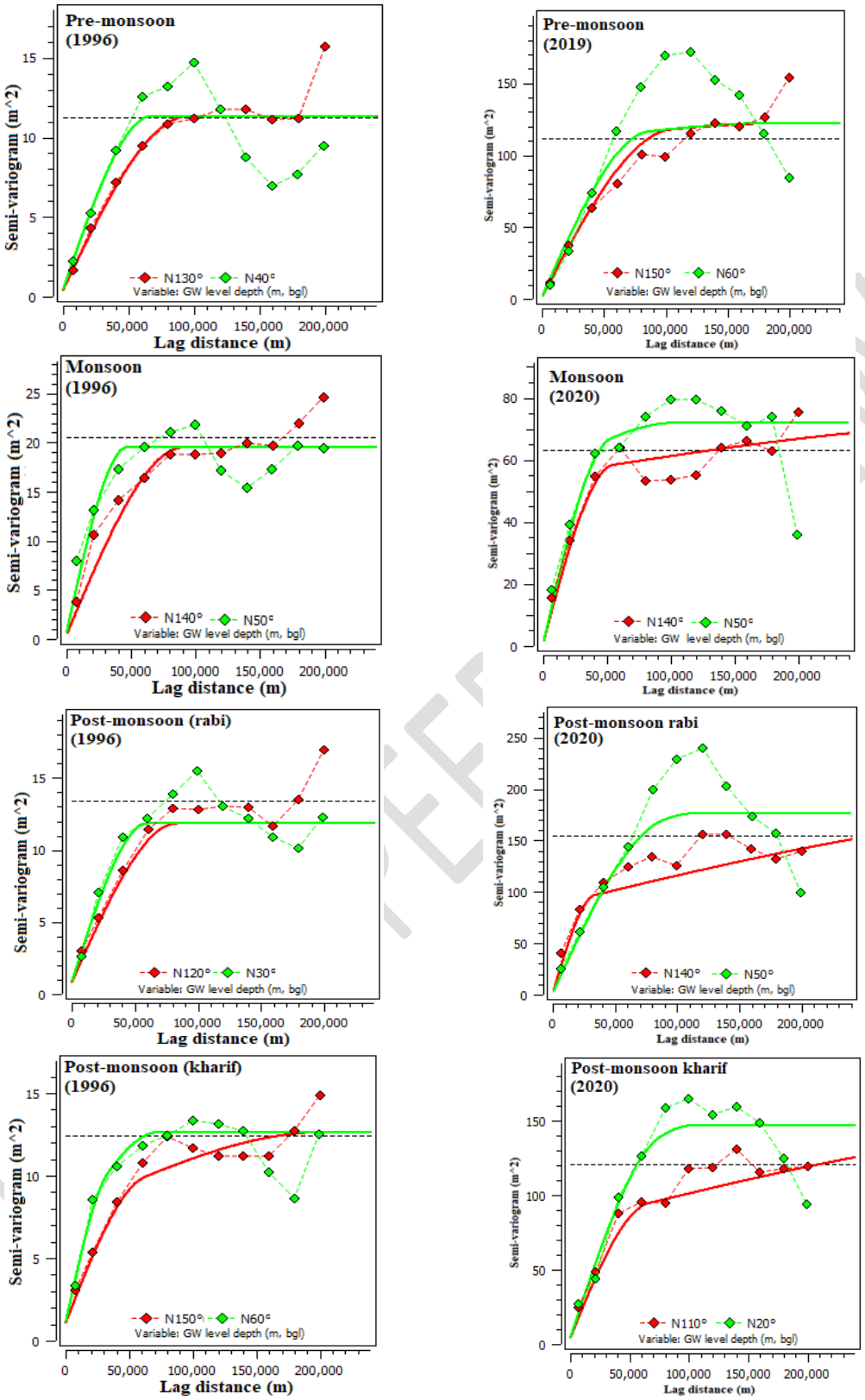

Figure 1 Anisotropic fitted semi-variogram model of groundwater (GW) level depth (m, bgl) for all four seasons

Table 1 (a) PKCV parameters for anisotropic spherical semi-variogram of groundwater level depth (GWD)

PKCV parameter of GWD for pre-monsoon season						PKCV parameter of GWD for monsoon season				
Year	Kriging Mean Error (m)	R^2	EV:KV	t-test on R^2	No. of Dug-well	Kriging Mean Error (m)	R^2	EV:KV	t-test on R^2	No. of Dug-well
1996	0.02	0.73	0.99	Sig.	263	-0.060	0.80	0.99	Sig	323
1997	0.03	0.71	0.95	Sig.	230	-0.020	0.70	1.03	Sig	317
1998	0.02	0.72	1.01	Sig.	146	-0.060	0.65	0.96	Sig	307
1999	0.02	1.00	0.95	Sig.	312	-0.010	0.70	0.96	Sig	222
2000	0.003	0.70	0.99	Sig.	304	-0.010	0.80	0.99	Sig	244
2001	0.008	0.73	0.95	Sig.	309	0.010	0.70	0.95	Sig	301
2002	0.05	0.72	0.97	Sig.	182	-0.010	0.70	0.96	Sig	113
2003	0.03	0.73	0.95	Sig.	215	0.010	0.80	0.96	Sig	253
2004	0.04	0.70	0.95	Sig.	205	0.030	0.72	0.97	Sig	248
2005	0.01	0.75	0.97	Sig.	223	0.003	0.80	0.98	Sig	237
2006	0.07	0.71	0.96	Sig.	195	0.020	0.80	0.97	Sig	204
2007	0.005	0.71	0.99	Sig.	236	***	***	***	***	***
2008	0.45	0.73	0.99	Sig.	210	-0.040	0.80	0.98	Sig	221
2009	0.09	0.70	0.96	Sig.	141	0.010	0.70	0.95	Sig	139
2010	0.03	0.65	0.96	Sig.	168	0.130	0.70	0.95	Sig	168
2011	0.09	0.65	1.02	Sig.	145	***	***	***	***	***
2012	***	***	***	***	***	***	***	***	***	***
2013	***	***	***	***	***	***	***	***	***	***
2014	0.14	0.61	0.97	Sig.	132	0.010	0.60	0.99	Sig.	85
2015	***	***	***	***	***	***	***	***	***	***
2016	***	***	***	***	***	***	***	***	***	***
2017	***	***	***	***	***	***	***	***	***	***
2018	0.04	0.66	1.01	Sig.	393	0.100	0.72	0.96	Sig	254
2019	0.005	0.80	0.95	Sig.	296	-0.140	0.80	0.96	Sig	247
2020	***	***	***	***	***	-0.060	0.80	0.99	Sig	323

*** -missing data & Sig.- significant

Table 1 (b) PKCV parameters for anisotropic spherical semi-variogram of groundwater level depth (GWD)

PKCV parameter of GWD for post-monsoon (rabi) season						PKCV parameter of GWD for post-monsoon (kharif) season				
Year	Kriging Mean Error (m)	R^2	EV:KV	t-test on R^2	No. of Dug-well	Kriging Mean Error (m)	R^2	EV:KV	t-test on R^2	No. of Dug-well
1996	0.06	0.80	0.95	Sig.	313	0.01	0.70	0.95	Sig.	328
1997	0.01	0.81	0.97	Sig.	327	0.003	0.80	0.96	Sig.	244
1998	0.04	0.70	1.05	Sig.	267	0.03	0.84	0.95	Sig.	214
1999	0.04	0.80	0.95	Sig.	294	0.02	0.70	0.99	Sig.	304
2000	0.01	0.70	1.03	Sig.	282	0.02	0.80	0.96	Sig.	236
2001	0.05	0.70	0.98	Sig.	199	0.06	0.70	0.99	Sig.	266
2002	0.05	0.80	0.98	Sig.	195	0.02	0.73	0.96	Sig.	181
2003	0.05	0.70	0.97	Sig.	258	0.01	0.80	0.96	Sig.	195
2004	0.04	0.71	0.99	Sig.	289	0.02	0.72	0.97	Sig.	230
2005	0.06	0.70	0.95	Sig.	210	0.01	0.80	0.96	Sig.	221
2006	0.01	0.70	0.97	Sig.	265	0.01	0.80	0.95	Sig.	217
2007	0.001	0.80	0.96	Sig.	222	0.08	0.70	0.96	Sig.	175
2008	0.01	0.73	0.98	Sig.	218	0.01	0.70	0.95	Sig.	143
2009	0.04	0.61	0.97	Sig.	149	0.10	0.70	0.99	Sig.	152
2010	0.03	0.70	0.99	Sig.	204	0.07	0.80	0.95	Sig.	150
2011	0.04	0.70	0.98	Sig.	212	0.10	0.70	0.96	Sig.	177
2012	***	***	***	***	***	***	***	***	***	***
2013	***	***	***	***	***	***	***	***	***	***
2014	0.16	0.61	0.99	Sig.	124	***	***	***	***	***
2015	***	***	***	***	***	***	***	***	***	***
2016	***	***	***	***	***	***	***	***	***	***
2017	***	***	***	***	***	0.14	0.70	0.96	Sig	200
2018	***	***	***	***	***	0.003	0.83	0.99	Sig	321
2019	***	***	***	***	***	***	***	***	***	***
2020	0.08	0.73	0.95	Sig.	179	0.11	0.80	0.95	Sig	432

*** -missing data & Sig.- significant

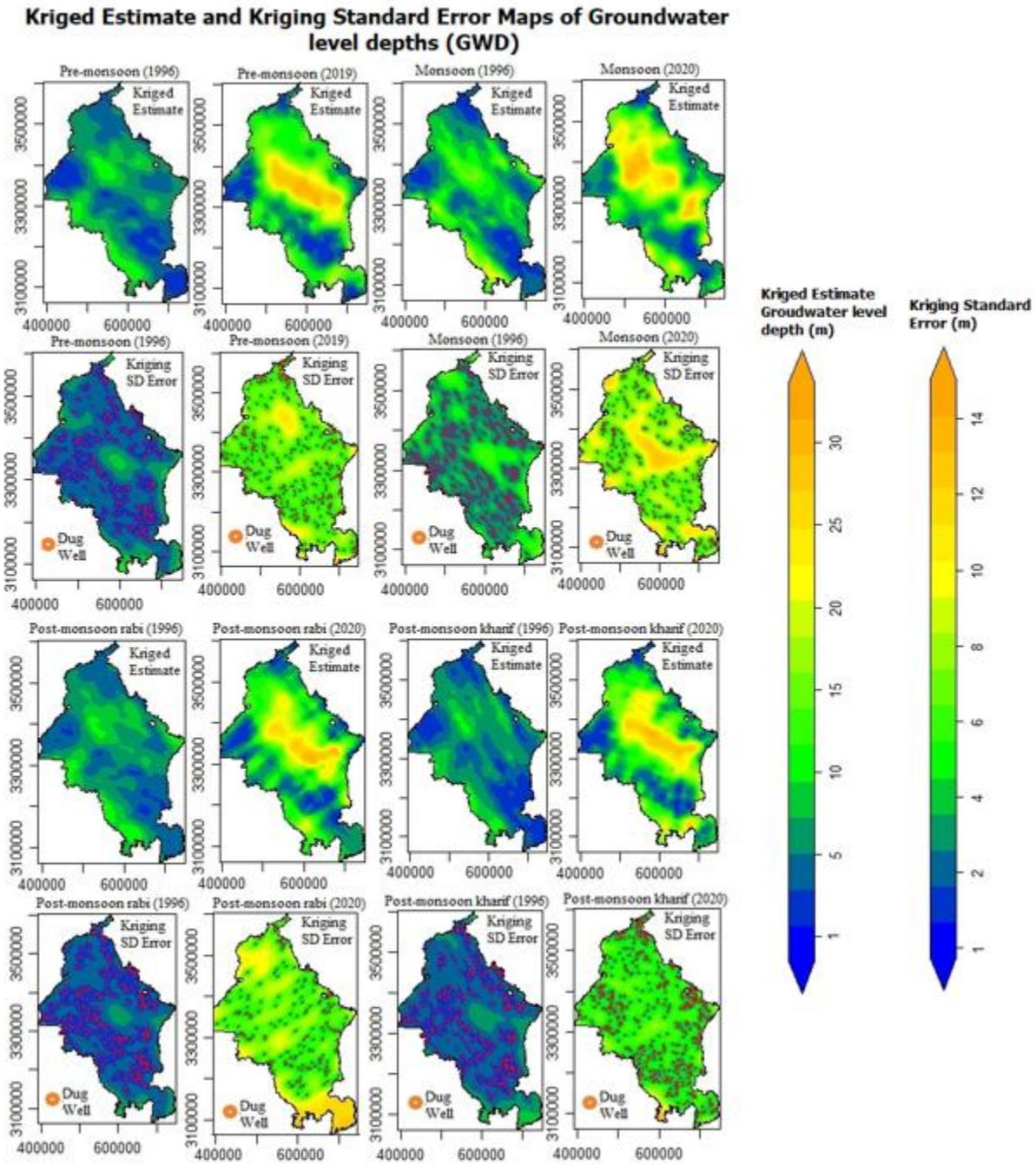

Figure 2 Kriged estimate and kriging standard error maps of groundwater level depth (GWD) for all seasons.

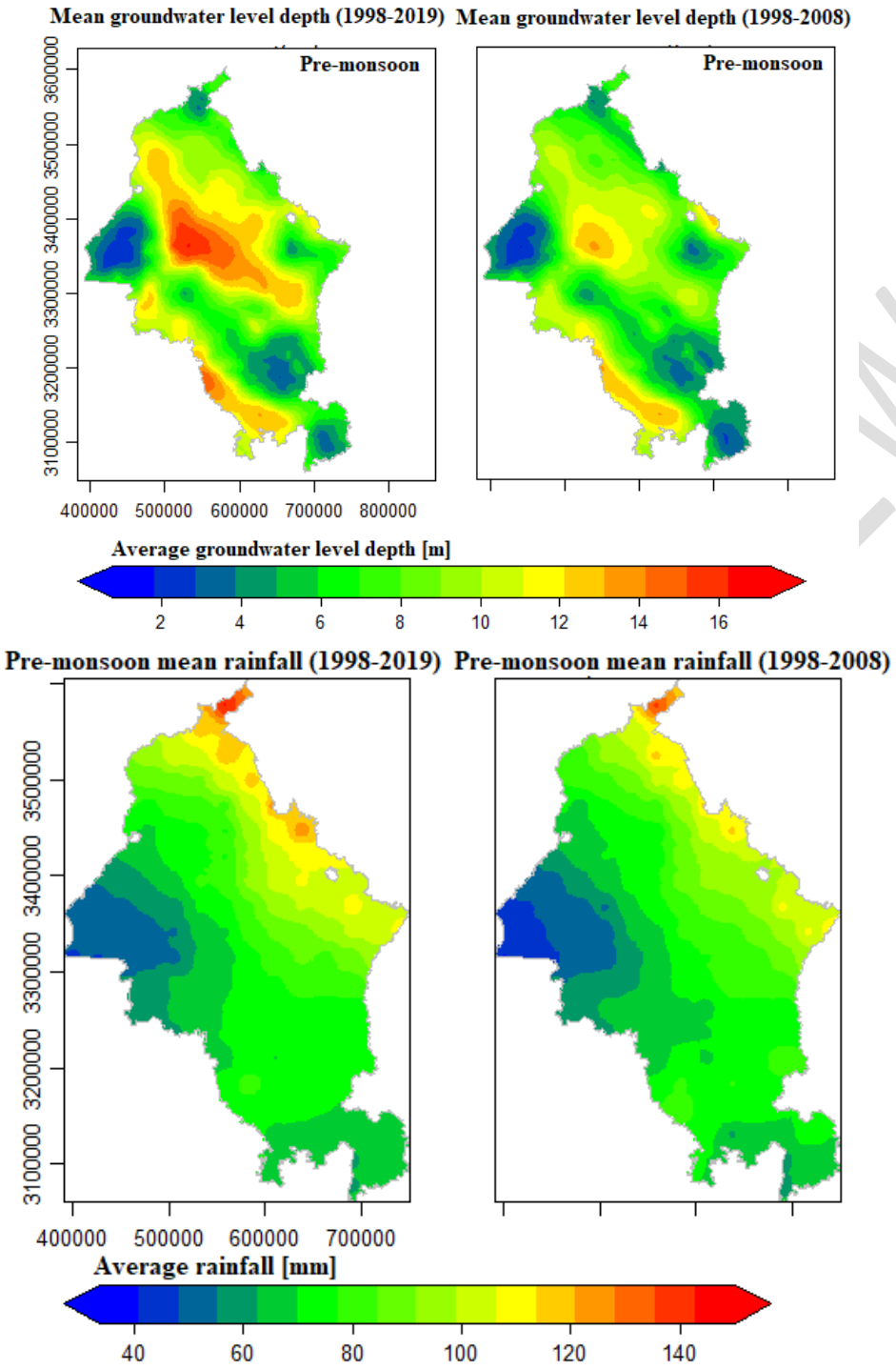

Figure 3(a) Mean kriged estimate of GWD and mean rainfall for pre-monsoon season in different time phases of 1998 to 2019 and 1998 to 2008.

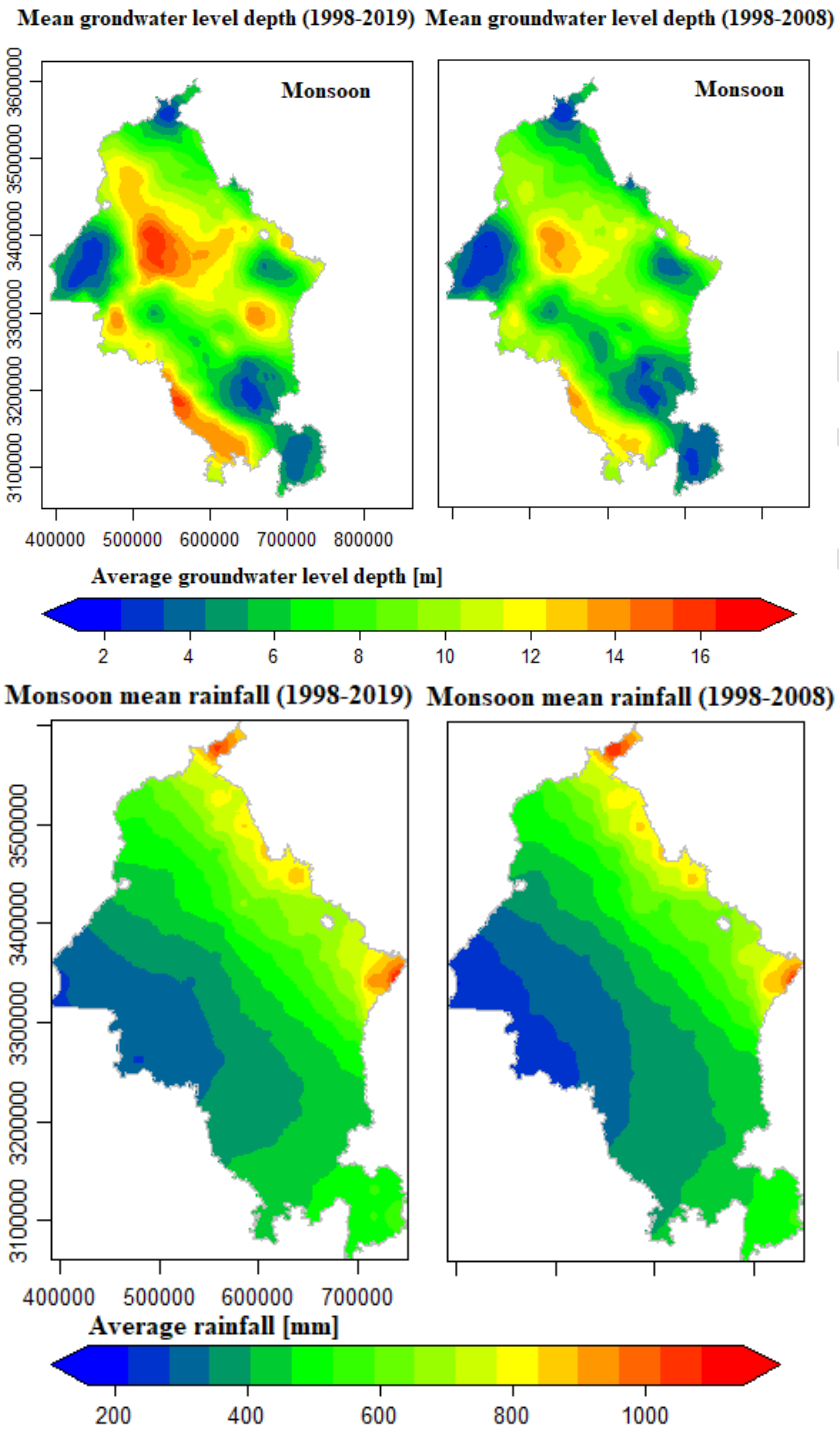

Figure 3(b) Mean kriged estimate of GWD and mean rainfall for monsoon season in different time phases (1998 to 2019 and 1998 to 2008).

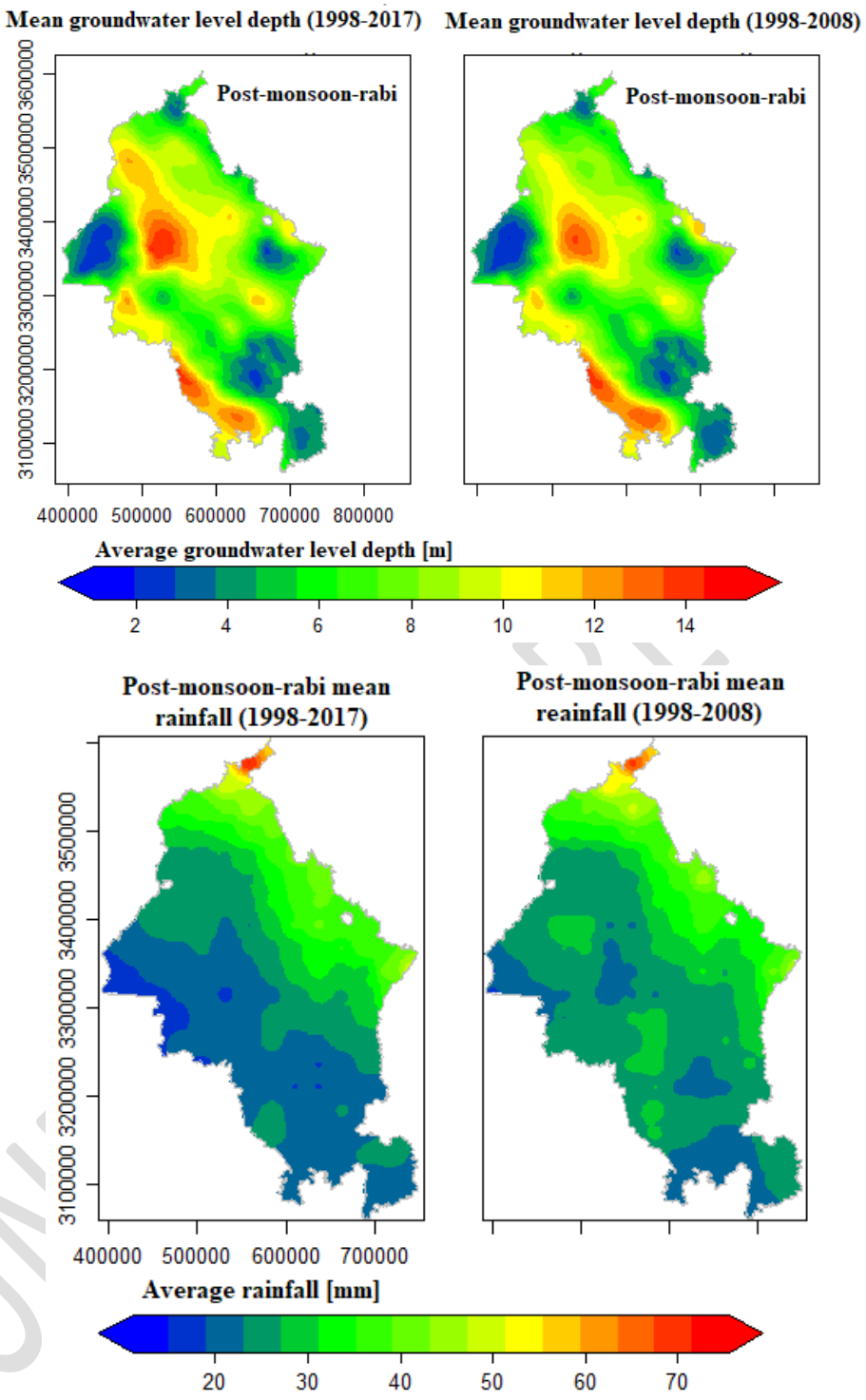

Figure 3(c) Mean kriged estimate of GWD and mean rainfall for post-monsoon-rabi season in different time phases (1998 to 2017 and 1998 to 2008).

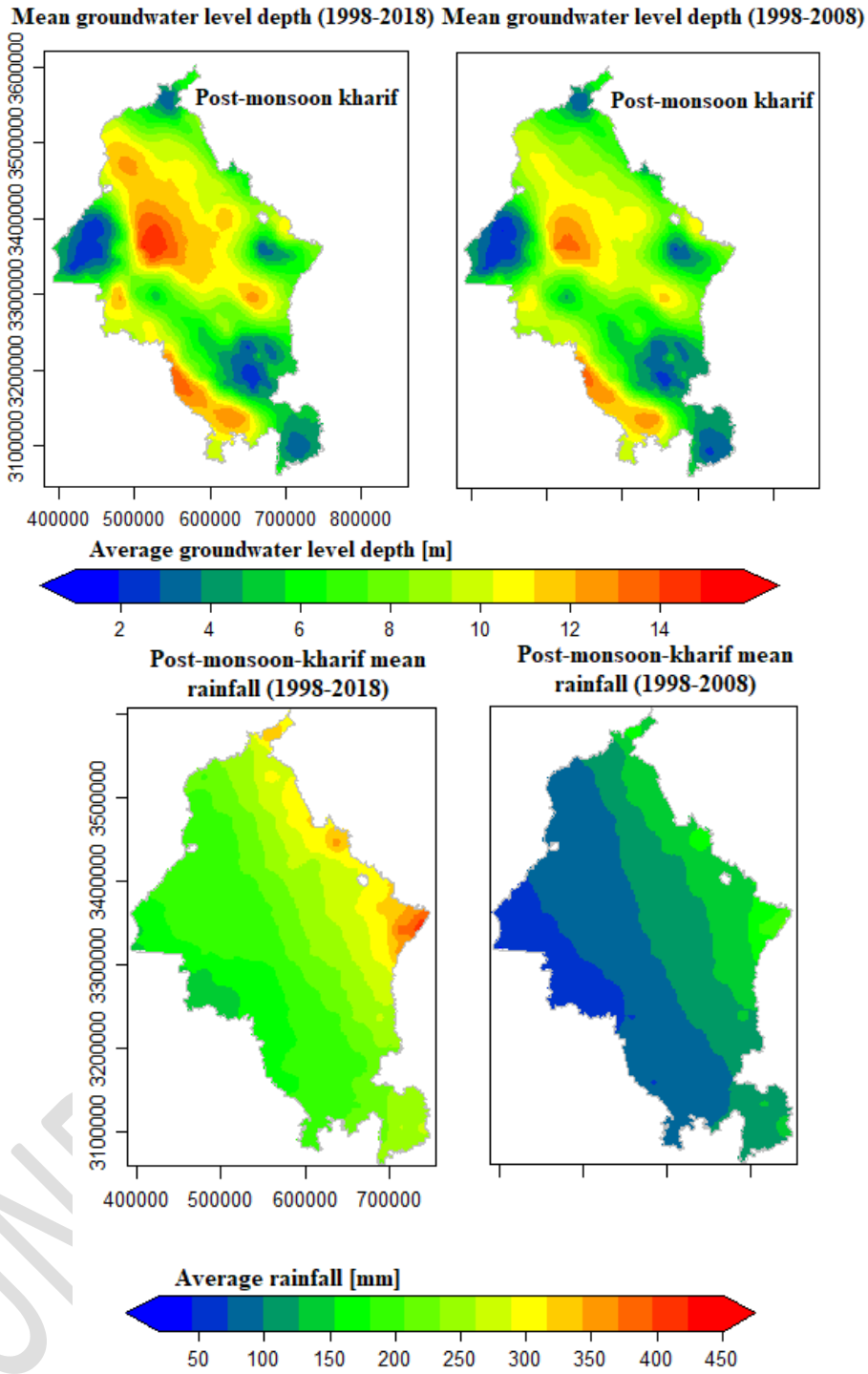

Figure 3(d) Mean kriged estimate of GWD and mean rainfall for post-monsoon-kharif season in different time phases (1998 to 2018 and 1998 to 2008).

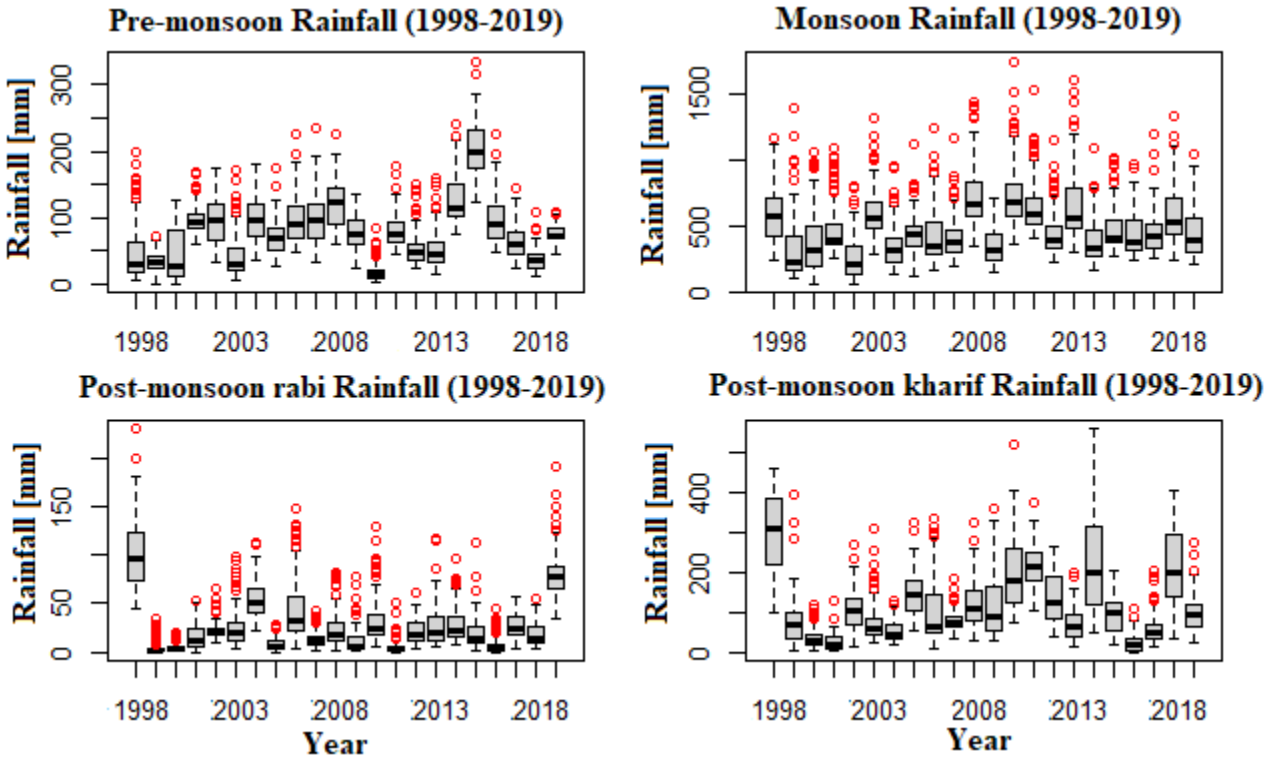

Figure 4(a). Box plots of input raw data of rainfall

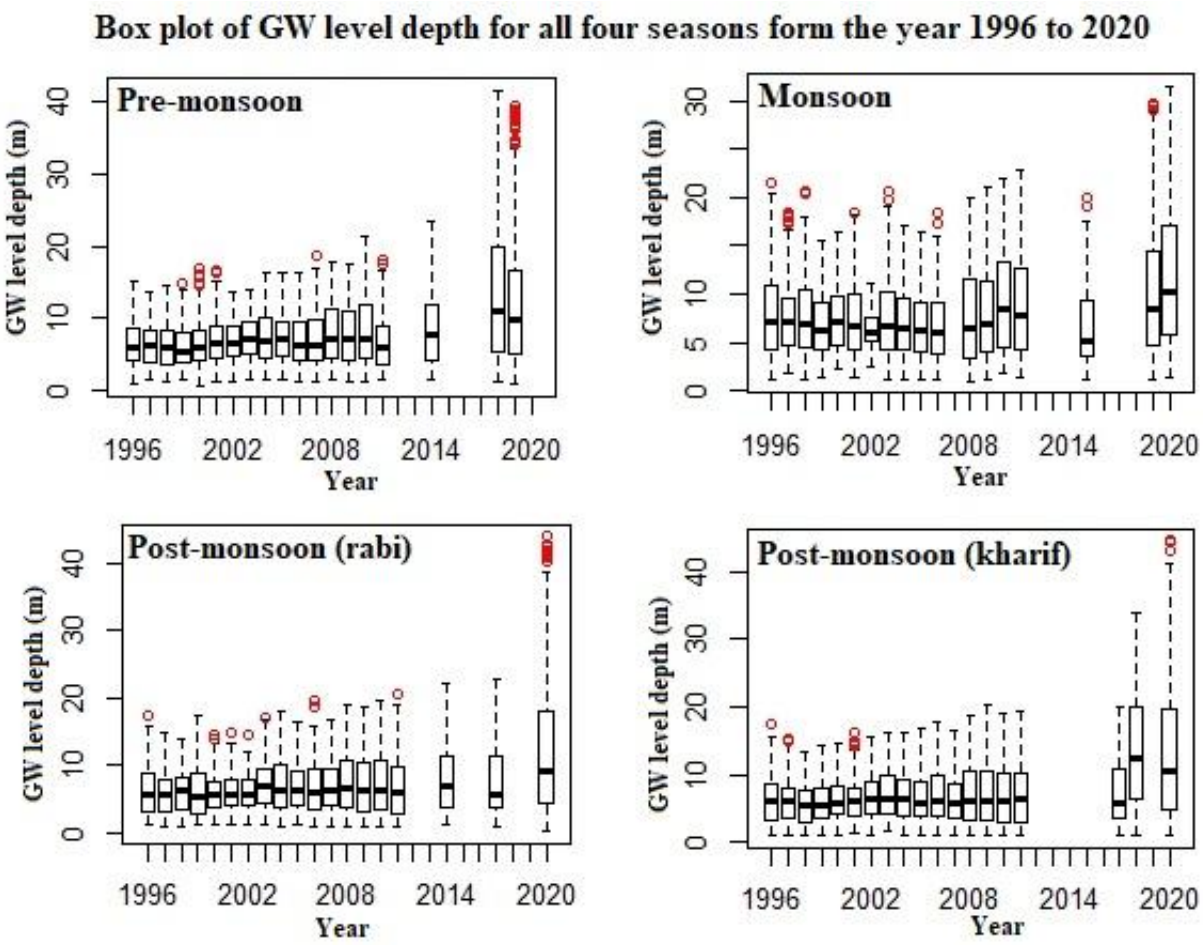

Figure 4(b) Box plots of input raw data of groundwater level depth (GWD)

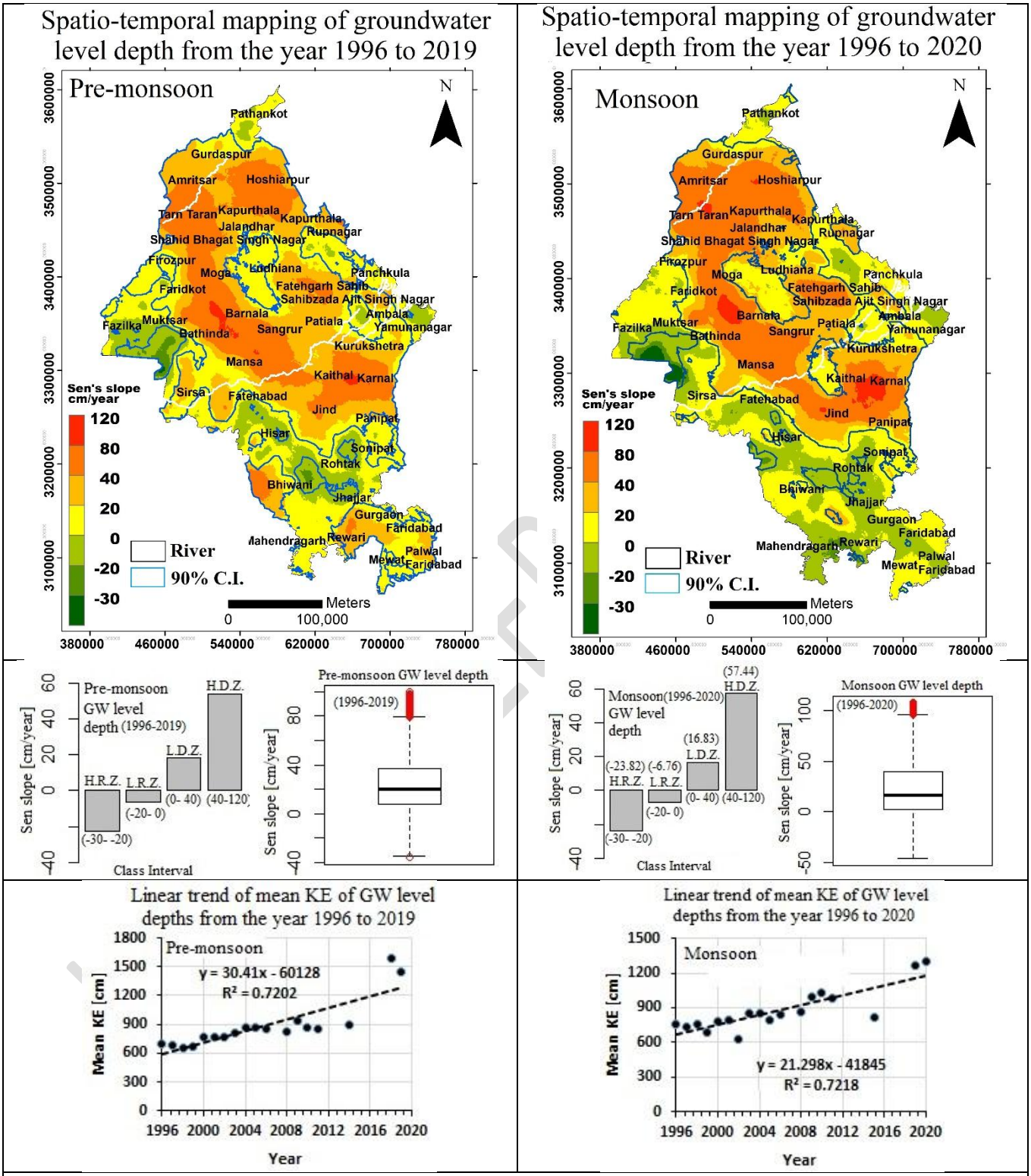

Figure 5a Trend mapping of GWD of pre-monsoon and monsoon seasons

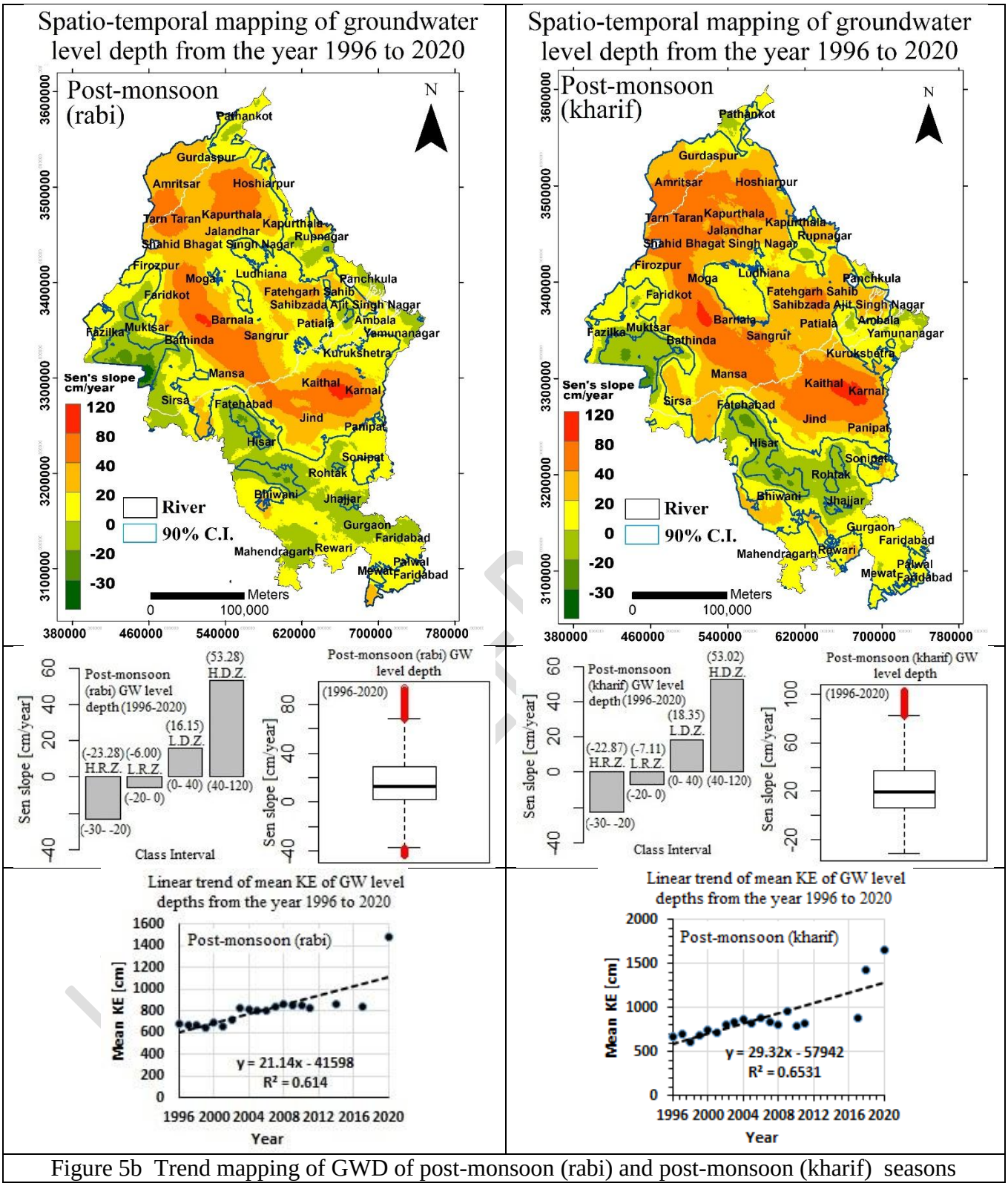

Figure 5b Trend mapping of GWD of post-monsoon (rabi) and post-monsoon (kharif) seasons